

PACS numbers: 78.67.-n; 42.65.-n; 42.65.Re
DOI: 10.1070/QE2013v043n04ABEH015119

Nanolocalised source of femtosecond radiation

T.V. Konstantinova, P.N. Melentiev, A.E. Afanasiev, A.A. Kuzin, P.A. Starikov, A.S. Baturin, A.V. Tausenev, A.V. Konyashchenko, V.I. Balykin

Abstract. **Possible spatial localisation of femtosecond laser radiation to the size on the order of 50 nm is studied. An approach to femtosecond laser radiation localisation in the nanometre scale is based on the use of nonlinear processes in metal nanostructures. It is shown that the extremely high third-order optical susceptibility of metal nanostructures and strong plasmon resonances give a possibility to realise an efficient nanolocalised source of radiation at the third harmonic frequency and a wideband femtosecond radiation based on metal photoluminescence.**

Keywords: *nanoplasmonics, nonlinear optics, harmonic generation, ultrafast photonics, light source.*

1. Introduction

The unique feature of femtosecond laser radiation is the time scale of localisation, which extends up to a single period of light. However, the spatial scale of localisation is not better than the radiation wavelength, which is explained by the diffraction limitation. In the present work we state the problem for femtosecond laser radiation to reach the spatial localisation of ~50 nm, which is of great fundamental and practical importance. Among important applied problems relevant to spatial localisation of light we may recall the possibility to combine modern silicon electronics with optical components (known as 'silicon photonics') and obtain short-wavelength laser radiation for optical lithography in a range 10–20 nm.

One approach to nanometre-scale spatial localisation of femtosecond laser radiation is employment of nonlinear processes occurring in metal nanostructures [1–3]. Possible nonlinear photoprocesses in metal nanostructures are based on three principal factors. These are the possibility to concentrate an electromagnetic energy in space with a characteristic nanometre-scale dimension by means of surface plasmons, an ultrashort (in the range 0.1–10 fs) relaxation time in metals, and available laser systems with ultrashort pulses capable of pumping optically a nanostructure for a femtosecond-scale time lapse.

T.V. Konstantinova, P.N. Melentiev, A.E. Afanasiev, V.I. Balykin Institute of Spectroscopy, Russian Academy of Sciences, Fizicheskaya ul. 5, 142190 Troitsk, Moscow, Russia;
e-mail: balykin@isan.troitsk.ru;
A.A. Kuzin, P.A. Starikov, A.S. Baturin Moscow Institute of Physics and Technology (State University), Institutskii per. 9, 141700 Dolgoprudnyi, Moscow region, Russia;
A.V. Tausenev, A.V. Konyashchenko Avesta Ltd., Fizicheskaya ul. 5, 142190 Troitsk, Moscow, Russia

Received 24 December 2012, revised 28 February 2013
Kvantovaya Elektronika **43** (4) 379–387 (2013)
Translated by N.A. Raspopov

Presently, various nonlinear photoprocesses are investigated in metal nanostructures, such as second harmonic generation [4, 5], four-wave mixing on metal surfaces [6], ultrafast optical modulation based on third-order nonlinearity [7–9], and generation of higher harmonics [10].

Unlike bulk media, harmonic generation in nanostructures does not necessitate the phase matching. Third harmonic generation (THG) is the simplest nonlinear effect allowed for nanostructures of arbitrary geometry, which is independent of their symmetry. It was theoretically shown [11] that under the radiation intensity of $\sim 10^{16}$ W cm^{-2}, the electric field amplitude of the third harmonic may be on the order of that of fundamental-frequency radiation.

THG was experimentally observed [12] under the action of a relatively weak light field of laser radiation (with the intensity of 10^{10}–10^{11} W cm^{-2}) on gold nanoparticles. To increase the process efficiency, the exciting field frequency in these experiments was equal to one third of the Mie-resonance frequency for the nanoparticle, that is, it was in resonance with the third-harmonic frequency. Nevertheless, the THG efficiency on nanoparticles was not high.

Optical antennas belong to the type of nanoparticles, in which an efficient nonlinear optical conversion is possible. It was shown [13] that nano-antennas may be efficient nonlinear sources of radiation. The possibility of creating a nano-scale radiation source is a goal of nanoparticle investigations. However, nanoparticles as the nano-scale sources of radiation have two substantial drawbacks. The first one is a high inherent background of the exciting radiation, and the second is nanostructure breakdown under a high power of incident radiation. The limitations on the pump radiation power result in a limited THG efficiency. There are nano-objects capable of generating third harmonic lacking these drawbacks, such as the nano-size hole in a metal film, which is the subject of our investigation.

Here we present the study of THG on single nanometre-scale objects such as circular or slit holes fabricated in gold and aluminium films. We have investigated the effect of film material and geometry on THG efficiency and the dependence of THG efficiency on the intensity of exciting laser radiation. The limitations were found on the utmost exciting radiation intensity that does not yet melt the nanostructure. The possibility is revealed of creating the nanolocalised source of third-harmonic radiation free of the background of exciting laser radiation. Also the possibility of generating a wideband femtosecond radiation based on metal photoluminescence is shown.

2. Experimental setup and measurement method

The possibility of creating a nanolocalised femtosecond radiation source was studied on the installation based on a Nikon

Eclipse Ti/U inverted microscope (Fig. 1). Laser radiation focused by an objective ($10^{\times}$, NA = 0.25) to the spot 4.3 μm in diameter in the plane of a sample was directed perpendicular to the surface of the film with nanoholes. Third harmonic and photoluminescence in metal nanostructures were excited by a femtosecond pulsed laser (with the radiation wavelength of 1560 nm, pulse duration of 120 fs, pulse repetition rate of 70 MHz, and average radiation power of incident radiation on the sample of 15 mW). The peak intensity of radiation on the sample was $\sim 1.1 \times 10^{10}$ W cm^{-2}. The zero-order $\lambda/2$ phase plate for the wavelength of 1560 nm was placed in front of the focusing objective to control the polarisation of the incident radiation. Signals of third harmonic and photoluminescence were collected by an objective ($40^{\times}$, NA = 0.65). The exciting radiation was suppressed by the set of interference and colour filters. In this way, the signal at the fundamental frequency was suppressed by more than 13 orders in magnitude. The spatial intensity distribution of radiation from nanostructures was detected by a cooled two-dimensional Photon-MAX CCD camera (Princeton Instruments) with avalanche electron multiplication. Spectral measurements were performed by the spectrometer with a cooled NTE/CCD-1340/100 CCD-matrix (Princeton Instruments). At the spectrometer input, the radiation was spatially filtered, which reduced the contribution of the background signal into the spectrum of detected radiation. The influence of mechanical perturbations was minimised by placing the unit on a vibroinsulated table.

The THG efficiency depends on third power of intensity at the fundamental frequency; hence, the position and dimension of the exciting radiation spot were thoroughly controlled relative to the position of the nanohole where THG was investigated. For this purpose, the nanohole was adjusted to the focused laser beam by means of the two-coordinate feedback-assisted table with CAP201XY piezoceramic actuators (Piezo Jiena), which provided a long-term control of the spatial position of the nanohole under test with an accuracy of ~10 nm. The spot dimension for the focused laser radiation was measured by spatially scanning the nanohole with a laser beam and detecting the radiation passed.

The absolute measurements of the power of third harmonic and luminescence require calibration of the 2D CCD-camera of the microscope. For this purpose the laser radiation at the wavelength of 1560 nm was directed to a nonlinear periodically poled $LiNbO_3$ crystal for obtaining third harmonic radiation. This radiation was directed to the microscope and then focused by an objective ($10^{\times}$, NA = 0.25) in order to illuminate the nanohole with a diameter of 400 nm, created in the aluminium film with a thickness of 100 nm. In this case, the signals at the fundamental frequency and at the frequencies of second and fourth harmonics were rejected by interference and colour filters. The radiation that passed through the nanohole was collected by an objective ($40^{\times}$, NA = 0.65) and detected by the 2D CCD-camera. The signal measured by the CCD-camera was calibrated by means of a commercial power meter.

The nanoholes and nanoslits were fabricated in the aluminium and gold films of nano-scale thickness deposited to a surface of ultrathin (40 nm) SiO_2 membranes [14]. Such membranes possess extremely low surface roughness (less than 1.5 Å), which, in turn, provides the high-quality surface of metal films from the side adjacent to the membrane. Thus, the contribution of luminescence (parasitic in our measurements) due to roughness of the metal surface is minimised: in all the measurements the more plain side of the film was faced to the exciting-frequency radiation.

Gold films were created by the method of thermal evaporation at the temperature of 1240 °C in high-vacuum conditions, aluminium films were produced by the electron-mean deposition method. The thickness of films was 50±5 nm which was tested on an atomic-force microscope. The samples were produced in the conditions of class 100 clean room, and optical measurements were performed in the conditions of class 1000 clean room.

Nanoholes of circular and slit shapes were studied. The diameter of nanoholes varied in the range 50–560 nm. Nanoslits with various length/width ratios had the area equal to

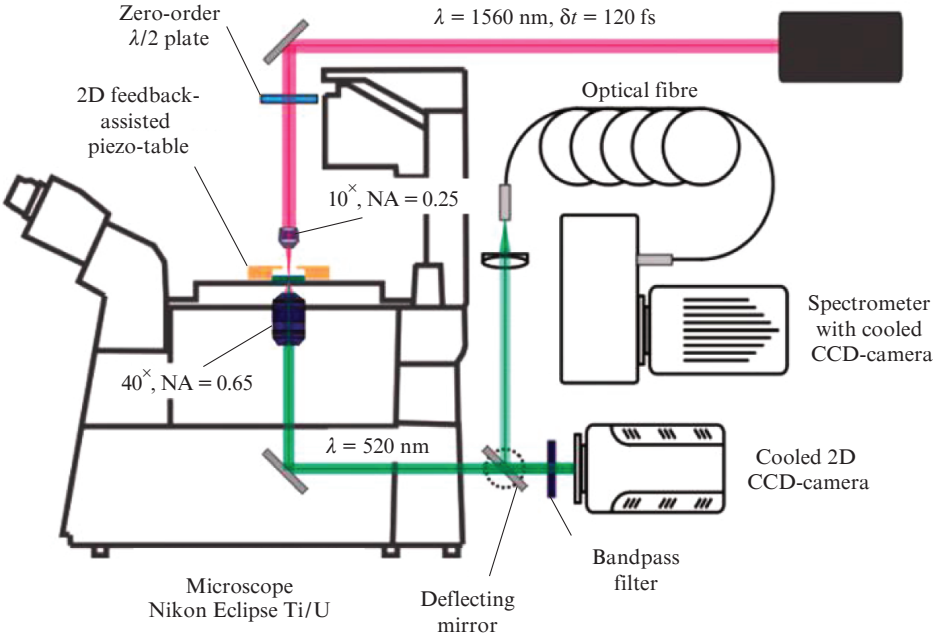

Figure 1. Experimental setup for studying localisation of femtosecond radiation in single nanoholes.

that of nanoholes. Thus, we might compare the THG efficiency on nanoholes and nanoslits.

Nanoholes were produced by the Ga^+ ion beam with the energy of 30 keV on a FEI Quanta 3D installation. The beam was focused to the spot with a diameter of ~10 nm. The nanoholes were tested by a JEOL JSM-7001F electron microscope with a spatial resolution of 5 nm at a relatively low beam energy (~5 keV). In this way we substantially reduced the parasitic carbon deposition on surfaces of metal films accompanying the electron microscopy of metal surfaces.

As an example, images of typical samples with nanoholes and nanoslits used in our investigation are presented in Fig. 2. In order to avoid an influence of collective plasmon effects the separation between nanoholes was taken 5 μm. It was also greater than the diameter of fundamental-frequency laser radiation spot. The series of produced nanoholes provided their identification and further operation with each hole separately.

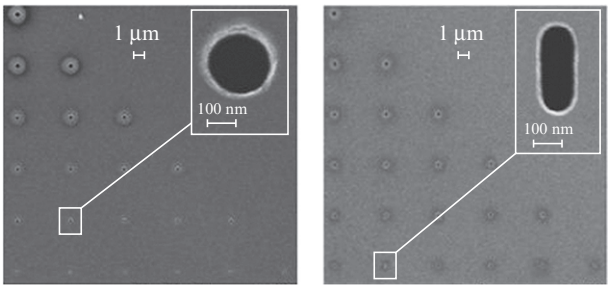

Figure 2. Nanohole images of (a) circular and (b) slit-like form in the aluminium film with the thickness of 50 nm, obtained by an electron raster microscope. Enlarged images are shown in the insets.

3. Source of femtosecond nanolocalised radiation based on THG on nanoholes

3.1. Nonlinear properties of metal films

Polarisation induced in medium under the action of field $E(t)$ is described by the expression [15]:

$$P(t) = \varepsilon_0(\chi^{(1)}E(t) + \chi^{(2)}E^2(t) + \chi^{(3)}E^3(t) + ...), \quad (1)$$

where $\chi^{(i)}$ is the ith order nonlinear susceptibility. In view of the vector character of field $E(t)$, the nonlinear susceptibilities of first, second, and third orders are tensors of second, third, and fourth orders, respectively. The term $P^{(3)}(t) = \varepsilon_0\chi^{(3)}E^3(t)$, which describes the nonlinear polarisation of the medium is responsible for third harmonic generation and describes the nonlinear polarisation of the medium, which in the case of the monochromatic exciting wave $E(t) = E_0\cos(\omega t)$ has the form:

$$P^{(3)}(t) = \frac{1}{4}\varepsilon_0\chi^{(3)}E_0^3\cos(3\omega t) + \frac{3}{4}\varepsilon_0\chi^{(3)}E_0^3\cos(\omega t). \quad (2)$$

Expression (2) describes the system response to the action of the field at frequency ω and to arising generation at frequency 3ω. The process efficiency is determined by the susceptibility $\chi^{(3)}$:

$$\chi^{(3)} = \frac{\chi^{(1)}(3\omega)E(3\omega)}{E^3(\omega)}. \quad (3)$$

For the films chosen with the thickness much less than $\lambda/4\pi$ the contribution into the nonlinear susceptibility from the dielectric–metal interface dominates over that from the bulk film material [15]. Thus, in view of expression (3) one can determine the nonlinear coefficient $\chi^{(3)}$ from the intensity measurements at the fundamental frequency $I(\omega)$ and at the third harmonic frequency $I(3\omega)$ [16]; in this case, the field in metal is determined by the following expressions:

$$E(\omega) = \left|\frac{2}{n(\omega)+1}\right|\left(\frac{2I(\omega)}{\varepsilon_0 c}\right)^{1/2}, \quad (4)$$

$$E(3\omega) = \left|\frac{n(3\omega)+1}{2n(3\omega)}\right|\left(\frac{2I(3\omega)}{\varepsilon_0 c}\right)^{1/2}\exp\left[\frac{\alpha(3\omega)}{2}\delta h\right], \quad (5)$$

where $n(\omega)$ is the complex refractive index of the metal film; δh is the film thickness; $\alpha(3\omega)$ is the damping coefficient for radiation at the frequency 3ω in the metal film [$\alpha_{Au} = 0.047$ nm^{-1} ($\lambda = 520$ nm), and $\alpha_{Al} = 0.15$ nm^{-1} ($\lambda = 520$ nm)]. The factors at the square root in expressions (4) and (5) are the Fresnel amplitude transmission coefficients for the film.

For studying the influence of material (Au and Al) properties of the films with nanoholes and nanoslits on the nonlinear properties of these nano-objects we first investigated the corresponding nonlinear properties of the materials themselves. The exciting laser radiation was focused to a surface of metal films. The third harmonic generated in this case was detected by the 2D CCD-camera as the radiation at the frequency of this harmonic passed through the film. The diameter of the focused laser spot was ~2 μm. The radiation at the third harmonic frequency was detected by the 2D CCD-camera as a spot 2.5 μm in diameter, which is less by a factor of $\sqrt{3}$ than the diameter of the focused radiation at the fundamental frequency due to a cubical dependence of the signal of third harmonic on the radiation intensity at the fundamental frequency.

In the spectra measured, the signal at the frequency of the third harmonic for the 50-nm-thick aluminium film was approximately five times greater than for the gold film of the same thickness (the films had no holes). The calculations performed with data from [17, 18] show that a transmission of the gold film at the wavelength of 520 nm is greater than that of the aluminium film by a factor of 700. This means that the THG efficiency in aluminium is substantially (by several orders) higher than that in gold. The absolute values of the third harmonic radiation power are: $P_{Au} = 2\times10^{-15}$ W, $P_{Al} = 9.8\times10^{-15}$ W. By using the coefficients of linear susceptibility $\chi^{(1)}_{Au}(3\omega) = -4.17 + 3.2i$ [17] and $\chi^{(1)}_{Al}(3\omega) = -39.2 + 10.9i$ [18] we obtain the coefficients of nonlinear susceptibility $\chi^{(3)}_{Au} = (2.3\pm0.7)\times10^{-20}$ m^2 V^{-2} and $\chi^{(3)}_{Al} = (2.6\pm0.8)\times10^{-17}$ m^2 V^{-2}. In the calculations, the laser pulse shape at the fundamental frequency was assumed Gaussian with the duration of 120 fs and at the third harmonic frequency it was taken also Gaussian with the duration of $120/\sqrt{3}$ fs. Note that in bulk samples at the wavelength of 1.5 μm the cubic optical nonlinearity may be measured by other methods not employing high-intensity radiation [19, 20].

The ratio of third-order nonlinear susceptibilities for gold and aluminium measured in the present work at the wavelength of 1.56 μm is ~10^3. This discrepancy in the nonlinear properties between gold and aluminium can be explained by

their physical and optical properties: the size of nanocrystals of polycrystalline structures in aluminium films is ~80 nm, whereas in gold films it is about 20 nm. The energy structures of these metals also differ significantly.

3.2. Nanoholes as nonlinear elements

Plasmon resonances in metal nanostructures give a chance to noticeably enhance the THG efficiency as compared to metal film due to a local increase in the field amplitude in the vicinity of nanostructures. It was shown [21] that the maximal THG efficiency is attained if two resonances occur simultaneously: at the fundamental frequency and at the third harmonic frequency.

Influence of plasmon resonances on THG was experimentally demonstrated in a gold film with a large massive of nanoholes [22]. In this experiment, the maximal efficiency of radiation conversion to the third harmonic was attained under the resonance condition for the exciting radiation at the fundamental frequency. In the present work we for the first time demonstrate THG on single nanoholes and increase in the efficiency of the process due to the plasmon resonance at the third harmonic wavelength.

For single nanoholes with the diameter of 50–300 nm produced in a gold film, the plasmon resonance resides in the wavelength range 500–550 nm [23]. When such a nanohole is illuminated by the radiation with the wavelength of 1560 nm, the third harmonic frequency coincides with the plasmon resonance frequency in gold. Such a resonance leads to an increase in the THG efficiency from nanoholes as compared to the gold film without holes.

For the holes in an aluminium film the plasmon resonance occurs at the wavelength of 150 nm; hence, in exciting a nanohole in aluminium by the radiation with a wavelength of 1560 nm, plasmon resonance does not arise and the plasmon mechanism of increased THG efficiency is not realised. Figure 3 presents the measured spectrum of the radiation from the nanohole 150-nm in diameter in an aluminium film irradiated by femtosecond laser pulses at the wavelength of 1560 nm. The nanohole image obtained with an electron microscope is shown in the inset. The third harmonic signals are shown in Fig. 4 as a function of the hole diameter in gold and aluminium films.

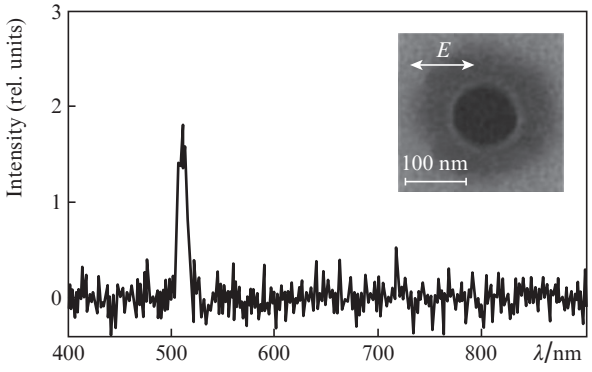

Figure 3. Radiation spectrum of the single nanohole in an Al film excited by the femtosecond laser radiation at the wavelength of 1560 nm. The hole image obtained by electron microscope is shown in the inset. Here and in Figs 5 and 6 the arrow denotes the electric field direction of exciting radiation.

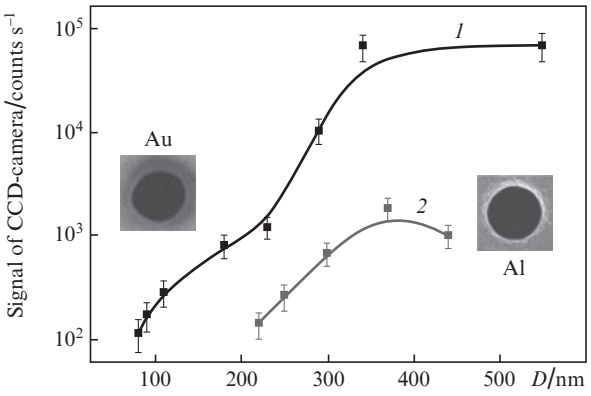

Figure 4. Intensity of third harmonic radiation as a function of diameter D of nanoholes produced in (*1*) gold and (*2*) aluminium films with the thickness of 100 nm.

The maximal THG efficiency obtained experimentally on the nanohole with 150-nm diameter in a gold film is 8×10^{-10}. One can see that the intensity of third-harmonic radiation for holes in the gold film is an order of magnitude greater than that for similar holes in the aluminium film. This is explained by the plasmon resonance arising in the gold film with a nanohole at the wavelength of THG (Fig. 5).

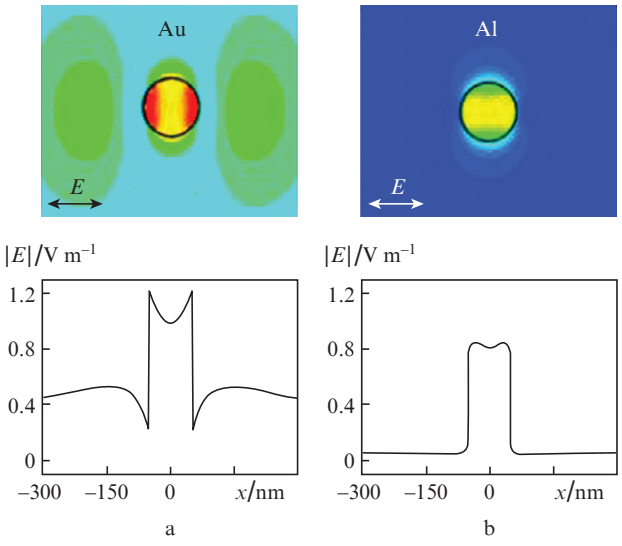

Figure 5. Calculated spatial distributions of the electric field amplitude at the wavelength of 520 nm near the hole with the diameter of 100 nm in 50-nm-thick (a) gold and (b) aluminium films.

Note that there is the problem of introducing the coefficients characterising optical nonlinear susceptibility for the nano-objects in the form of nanoholes. At various points of the film with the hole the radiation at the third harmonic wavelength is formed by the fundamental-frequency field of different amplitudes. Near the hole the field is strong but occupies a small volume. At a distance from the hole the fields are weaker but occupy a large volume so that the contribution into the nonlinear signal is also noticeable and may even dominate. However, high enhancement of the local field by the nanostructure, strong cubic dependence of THG efficiency on the amplitude of the exciting field at the fundamen-

tal frequency, tight focusing of laser radiation on a sample, and confocal geometry of the signal detection scheme result in that the signal in the experiments can only be detected from the nanohole.

3.3. Nanoslit as a nonlinear element

Unlike a nanohole, the nanoslit made in a metal film may have several resonances rather than one, because the resonance frequency is determined not only by the optical properties of the film material and its neighbourhood but also by the nanoslit geometry [24]. As was reported [25] the choice of nanostructure geometry may help one to realise the resonance conditions both at the exciting frequency and at that of second harmonic. This, in turn, substantially increases the second harmonic generation efficiency. The double resonance may also be employed for increasing the THG efficiency on nanostructures including nanoslits.

Our calculations show that the resonance at a wavelength of 1.56 μm in the nanoslit in the aluminium film is realised when the slit length is ~600 nm. The slit with such length is not interesting from the viewpoint of creation of the radiation source with nanometre spatial localisation and we did not investigate this case. However, a plasmon resonance can be excited at the third harmonic wavelength ($\lambda = 520$ nm) on the nanoslit of length shorter than 200 nm. This dimension is certainly interesting for designing a radiation source with nanometre spatial localisation. In the present work this resonance was excited for increasing the THG efficiency on a single nanoslit.

The optimal nanoslit geometry was determined from the computer simulation by the FIT (Finite Integration Technique) approach of slit transmittance for the field presented by the plane monochromatic wave ($\lambda = 520$ nm) corresponding to THG with the wave vector normal to the slit plane. The vector of the field of incident radiation was orthogonal to the 'long' axis of the slit. The calculations show that the plasmon resonance arises at the third harmonic wavelength ($\lambda = 520$ nm) at the slit length of ~170 nm.

We have made a series of nanoslits of size 50–170 nm in an aluminium 50-nm-thick film. Results of THG obtained on such a slit are presented in Fig. 6. One can see that the distribution of radiation intensity for third harmonic consists of two parts: the wide pedestal related with THG in the metal film and the narrow diffraction-limited peak caused by THG on the nanoslit. One can also see that if the polarisation of incident radiation corresponds to excitation of plasmon resonance (the polarisation along the shorter axis of the slit) then the signal of third harmonic is much higher than with the orthogonal polarisation where the plasmon resonance is not excited. Similar signal relations were obtained with other slits of the same geometry. The THG efficiency was $\sim 10^{-9}$. The corresponding generation efficiency for the slit of the same geometry made in the 50-nm-thick gold film was $\sim 7\times 10^{-10}$.

We investigated the influence of the film material on the THG efficiency by experimenting with slits of various lengths (from 50 to 300 nm) in aluminium and gold films. The efficiencies measured confirmed the resonance properties for the slit of size 50×170 nm in aluminium foil. No resonances related with the slit geometry were found in the gold film.

In a separate experiment we compared the THG efficiencies on circular holes and nanoslits having equal areas and different hole dimensions and nanoslit geometries. The efficiencies of THG measured for circular holes and nanoslits made in the gold film were approximately equal. In the case of aluminium film the ratio was quite different: the signal of THG from a nanoslit was almost 20 times that from a circular hole. This fact confirms the contribution of plasmon resonance into the THG efficiency.

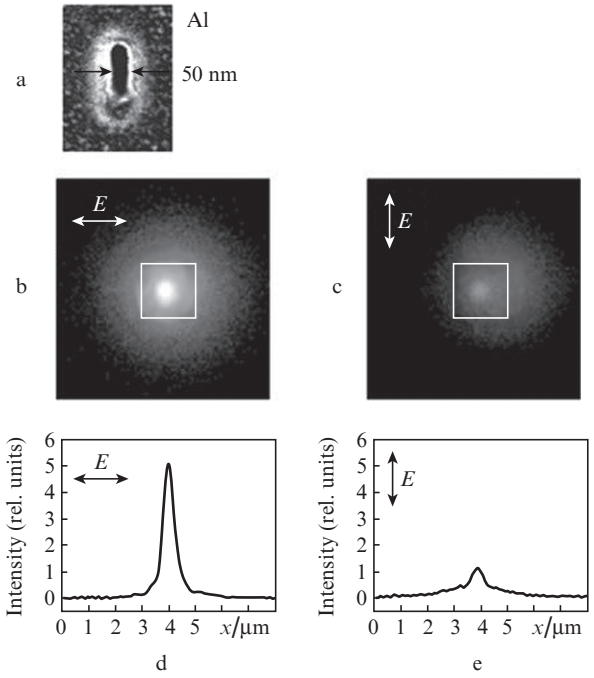

Figure 6. THG on the nanoslit of size 50×170 nm made in the 50-nm-thick aluminium film. (a) The slit image obtained by the electron microscope and the image at the third harmonic wavelength obtained by an optical microscope when the polarisation of exciting radiation is per(b) pendicular or (c) parallel to the slit axis; panels (d) and (e) show the corresponding intensity distributions.

3.4. Comparison of nonlinear properties of gold and aluminium from the viewpoint of fabricating an intense nanolocalised source of third-harmonic radiation

Gold is a basic material for creating elements employed in nanoplasmonics. However, it was recently shown [26] that in some cases aluminium has certain advantages over gold because it exhibits stronger nonlinear properties. Experiments with aluminium [26] were carried out at the wavelength of 780 nm, which fits the aluminium absorption band. In the present work, the frequency of the exciting radiation with the wavelength $\lambda = 1560$ nm is far from frequencies of band-to-band electron transitions in aluminium, which gives a hope for stronger nonlinear properties of aluminium in this frequency range.

Nonlinear properties of aluminium and gold were compared by the THG efficiency on various nanostructure objects. As was mentioned, the efficiency depends not only on the material comprising the nano-objects but on their geometry, which in certain cases favours realisation of plasmon resonances in the nanostructures. The measurements performed in the present study show that in the nano-objects having the form of thin films, the main factors affecting the THG efficiency are nonlinear properties of the film material.

This is why the THG efficiency in aluminium is noticeably higher than in gold.

In nanoholes, a plasmon resonance may arise, which increases the local field, which, in turn results in a higher THG efficiency. The frequency of such resonance depends on the material of the film comprising the hole and is independent of the hole geometry. As is known, the plasmon resonance on nanoholes in a gold film arises at wavelengths of 500–600 nm, whereas no resonances occur on nanoholes in an aluminium film in this wavelength range. The THG efficiencies on nanoholes in aluminium and gold films measured in our experiments show that the effect of plasmon resonance on a gold nanostructure dominates the effect of nonlinearity in aluminium, which is stronger than that in gold.

Nano-objects in the form of slits in an aluminium film allow one to realise the plasmon resonance at the third harmonic wavelength, which will be sensitive to the polarisation of laser radiation as well. Due to stronger nonlinear properties of aluminium as compared to gold the THG efficiency on slits in aluminium was higher and equal to $\sim 6\times10^{-10}$ under the plasmon resonance conditions.

A higher efficiency may be achieved by increasing the radiation intensity at the fundamental frequency [11] because the value of nonlinear dipole momentum induced in the nano-object at triple frequency is proportional to the third power of the incident field amplitude.

Main objects in nanoplasmonics are nanoparticles and their complementary nanoholes. According to Babinet's principle, the optical properties of nanoparticles and complementary nanoholes are similar. Hence, both nanoparticles and nanoholes can be used for fabricating nanolocalised radiation sources. As was already shown above, nanoparticles and nanoholes may serve as nonlinear sources of radiation. The sources of exciting radiation have high intensity, which leads to heating and the following change in the geometrical form of metal nanostructures and, consequently, in their resonance properties. In this case, a dramatic change in the optical properties of the nanostructure occurs, in particular, the efficiency of nonlinear processes substantially falls. We have investigated these processes.

It was shown [10–12] that high-intensity radiation acting on gold nanostructures causes their intensive heating, resulting in melting and shape changes. Such changes occur at the radiation intensities above 10^{10} W cm^{-2}. We investigated the heating of nanostructures (both nanoparticles and nanoholes) under the action of high-intensity radiation.

We calculated the temperature distribution in the aluminium disk of diameter 570 nm and thickness 50 nm (by the FIT method) and similar distribution in the nanohole of the same size made in the 50-nm-thick aluminium film. Both the structures were illuminated by a plane monochromatic wave with the wavelength of 520 nm and the wave vector orthogonal to the nanostructure plane. The radiation intensity was 8×10^{13} W cm^{-2} and the wavelength chosen was beyond the range of plasmon resonances. The calculations showed that the temperature increases locally near the nanostructures. In this case, the absolute values of temperature were moderate and comparable for both the nanodisk and nanohole.

Quite different temperature distribution is realised in nanostructures excited by the radiation at the frequency coinciding with those of nanostructure plasmon resonances. The nanodisk was heated to a higher temperature than the nanohole. A strong plasmon resonance in gold at the exciting wavelength leads to strong local fields and, consequently, to intensive local heating. Conversely, in the case of a nanohole the heat is efficiently withdrawn by the metal film surrounding the hole, which provides a lower local temperature than in the nanodisk placed on the dielectric material with low thermal conductance. Thus, the metal melting temperature is reached in the nanodisk at a lower laser radiation intensity than in a nanohole. This, in turn, suggests a higher THG efficiency on a nanohole than on a nanodisk of the same geometry.

4. Source of femtosecond nanolocalised radiation based on photoluminescence from nanoholes

We have also studied the possibility of designing the nanolocalised source of femtosecond radiation based on photoluminescence (PL) in metal. The process of radiation absorption in metal with following PL is only possible on the scale of a skin-layer, that is, on nano-dimension scales. With progress in the production methods for nanostructure objects, the interest to PL revived in the field of nano-size structures. The efficiency of PL for spherical nanoparticles is $\sim10^{-6}$ [27], whereas in the case of nano-rods it may reach 10^{-4} [28]. The PL efficiency in molecular clusters may be tens of percent. The mechanism of a high increase in the PL efficiency in gold nano-objects is explained by an optical excitation of band-to-band d–sp transition, the following recombination of the d-band hole with the sp-electron, and emission of a photon by a nanoparticle plasmon [29]. A further increase in the PL efficiency is possible in nano-objects having the shape of nanorods, where the electric fields of incident and emitted radiation are amplified by plasmon resonance effects [28, 30, 31].

We have investigated PL of a single nanohole and found an extremely wide band of nanohole PL and a considerable PL quantum yield. It was also shown that these two physical properties give the possibility to fabricate on this basis a nanolocalised wideband tunable nano-size source of radiation. We have demonstrated functioning of such a source by means of the microcavity based on the one-dimensional photonic crystal.

Choice of the nanohole as the nanolocalised source of radiation has an advantage over nanodisk in that the source can be realised without background. It is possible because in the case of a nanohole the background from the exciting radiation is lacking, whereas in the case of a nanoparticle (usually deposited on a dielectric surface), in addition to PL, there is intense exciting radiation and considerable background scattering from the surface. In addition, the breakdown threshold for nanoholes is substantially higher due to more efficient heat removal by the metal film comprising the hole, which admits higher intensities of exciting radiation.

The scheme of the experiment on studying PL from a single nanohole and creating on this basis a nanolocalised source of radiation is shown in Fig. 7a. The experiment was carried out as follows. The radiation of the diode laser (λ = 406 nm) was used for exciting band-to-band d–sp transitions in the gold film with a nanohole. The laser radiation with a power of 22 mW was focused by an objective (20$^{\times}$, NA = 0.45) to the surface of the sample with a nanohole placed on the objective stage of the Nikon Eclipse Ti inverted optical microscope. The laser beam diameter in the sample plane was 830 nm. The radiation of PL from the nanohole was focused by an objective (20$^{\times}$, NA = 0.45) from the opposite side of the gold film

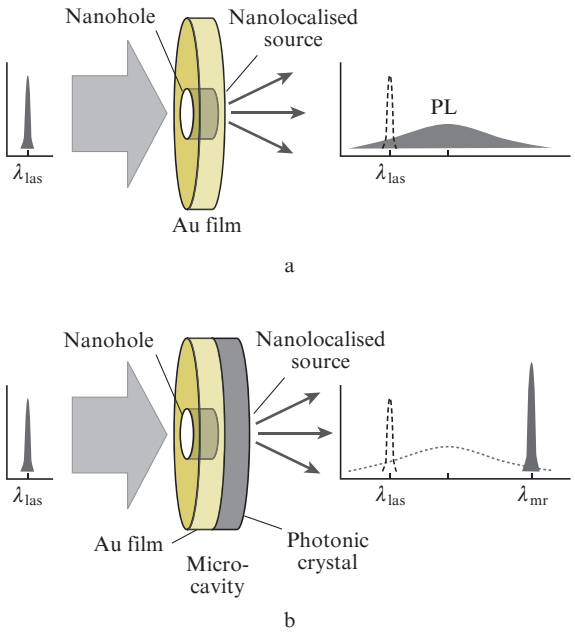

Figure 7. (a) Scheme of nanolocalised and wideband radiation sources based on metal PL, and (b) scheme of similar source with photonic crystal.

with a nanohole onto the two-dimension cooled CCD-array with avalanche electron multiplication (Princeton Instruments) or onto the entrance slit of the diffraction spectrometer with a cooled CCD line array (Princeton Instruments). The radiation at the fundamental frequency was suppressed by an interference barrier filter. The experimental setup was capable of obtaining 2D optical images of single nanoholes with the spatial resolution of ~1 μm and studying the emission spectrum in the wavelength range 480–825 nm with the resolution of ~1 nm. The samples were prepared in the conditions of class 100 clean room.

The nanoholes were produced by a tightly focused ion beam in the gold films of various thicknesses (50, 100, and 200 nm) deposited on a ultrathin (40 nm) SiO_2 membrane [14]. The nanohole diameter varied from 20 nm to 1 μm. Note that the measurements in the present work were performed with single holes. Each hole had a unique mark which provided identification of the holes on a gold film. The shape and dimension of the holes were measured by a JEOL JSM-7001F electron microscope with the spatial resolution of ~5 nm. The minimal separation between nanoholes was ~5 μm.

Employment of the ultrathin membrane as a substrate for the gold film has the following advantages: the gold film from the side adjacent to the membrane has a smooth surface due to a high quality of the membrane surface; the PL signal from the membrane due to its small thickness is three orders of magnitude lower than the luminescence signal from the smooth gold surface.

Due to localised plasmon oscillations excited on the nanohole, the intensity of gold luminescence near the nanohole exceeds that from gold surface by a factor of $\sim 10^4$; hence, the luminescence from the nanohole exhibits high spatial localisation.

The PL spectra from single nanoholes with the diameters of 65 and 560 nm produced in a 100-nm-thick gold film are presented in Fig. 8. The spectra were recorded by using the

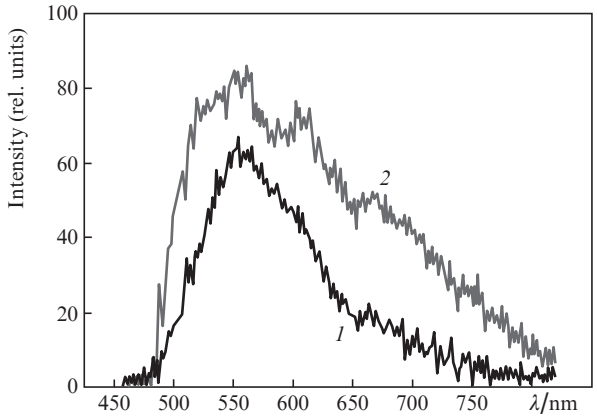

Figure 8. Spectra of PL from single nanoholes with the diameter of (*1*) 65 and (*2*) 560 nm produced in a 100-nm-thick gold film.

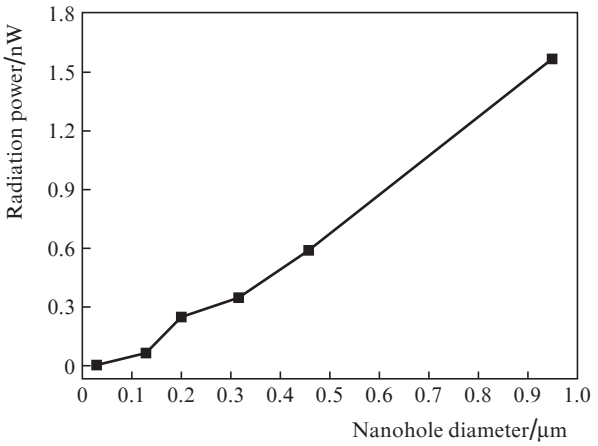

Figure 9. Wideband radiation (PL) power for a single nanohole in a 200-nm-thick gold film vs. the nanohole diameter.

interference barrier filter with the cut-off wavelength of 480 nm. One can see that the emission spectrum of the nanohole is continuous in the range 480–825 nm. The power of the wideband radiation (PL) from a single nanohole in the gold film of thickness 200 nm is shown in Fig. 9 versus the hole diameter. The power of the wideband radiation from a single nanohole is several nW. For the hole with the diameter of 200 nm the radiation power is 0.3 nW, and the radiation intensity near the nanohole is about 1 W cm^{-2}.

In the present work we have also realised the scheme for controlling spectral composition and efficiency of a localised light source by means of a 1D photonic crystal (see Fig. 7b). The photonic crystal deposited to a gold surface gives the possibility to realise a microcavity with the Q-factor of ~100. The radiation of the localised light source is amplified at the resonance wavelength of the microcavity, whereas radiation at other wavelengths is attenuated. We have demonstrated the control over the spectrum and efficiency of the nanolocalised light source [32, 33]. The microcavity was formed by an optically thick gold layer (200 nm) and twelve alternating dielectric layers of TiO_2 and MgF_2 of thickness $\lambda/4n$ (λ = 730 nm) differing in the refractive index. The refractive index of the TiO_2 layer was large (n = 2.23), whereas that of MgF_2 was small (n = 1.38). The twelve dielectric layers formed a one-

dimensional photonic crystal with low (~2%) light transmission in the spectral range 650–800 nm (the forbidden band of the photonic crystal).

The exciting laser radiation illuminated the nanohole with a diameter of 60 nm, forming in this way a spatially localised source of wideband radiation (PL) inside the microcavity. The PL spectrum from the nanohole with a 60-nm diameter in the 200-nm-thick gold film (without photonic crystal) is shown in Fig. 10a along with the calculated transmission spectrum for the nanohole of the same diameter made in the microcavity (in a gold layer). The narrow resonance in the transmission spectrum at the wavelength of 782 nm is the consequence of the fabricated microcavity with the Q-factor $Q \simeq 120$. Light attenuation in the spectral range 600–750 nm is related to low light transmission at the wavelength corresponding to the forbidden band of the photonic crystal. The experimental spectrum of radiation from the nanohole in the microcavity shown in Fig. 10b is in a good agreement with the calculated spectrum in Fig. 10a. Note that employment of the microcavity allows one to realise a 30-fold enhancement of the radiation power from the nanohole at the central frequency of the microcavity. The measurements performed in [34] revealed one more important feature of the 'nanohole + microcavity' object in the scheme shown in Fig. 7b: the radiation from the nanohole possesses directivity – it is concentrated in the cone with the total angle of ~60°.

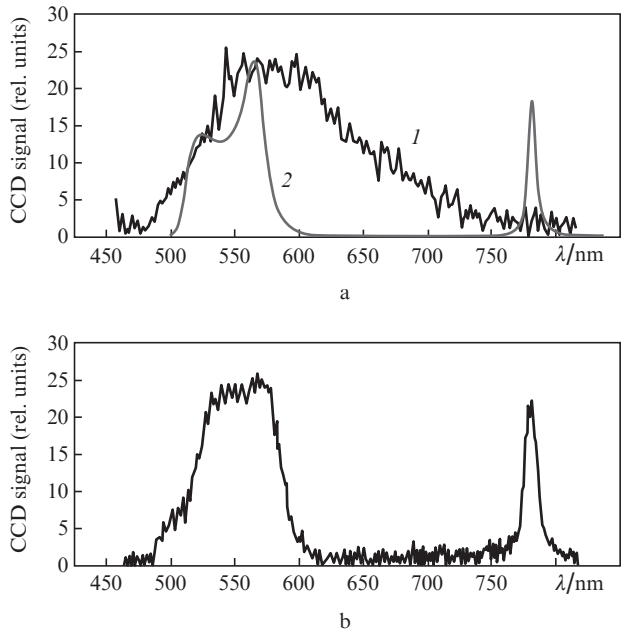

Figure 10. (a) PL spectrum of a nanohole with a diameter of 60 nm in a 200-nm-thick gold film (*1*) and calculated transmission spectrum for the nanohole in a microcavity (*2*) as well as (b) measured emission spectrum of a nanohole in a microcavity [34].

5. Conclusions

The possibility to spatially localise femtosecond laser radiation to the size ~50 nm is studied. Two approaches are realised to nanometre-scale localisation of femtosecond laser radiation: employment of nonlinear processes in metal nanostructures for THG and use of nonlinear processes in nano-objects for exciting photoluminescence. It was shown that extremely high third-order optical susceptibility in metal nanostructures and strong plasmon resonances allow one to realise an efficient nanolocalised source of radiation at the third harmonic frequency and a wideband femtosecond radiation based on metal photoluminescence.

Acknowledgements. The work was partially supported by the Russian Foundation for Basic Researches (Grant Nos 11-02-00804-a, 12-02-00784-a, 12-02-33073) and the programme 'Extreme Light Fields and Their Applications' of the Presidium of the Russian Academy of Sciences The work was performed by employing equipment from the Shared Research Centre of ISAN, the Shared Research Centre of MIPT (project No. 16.552.11.7022), the Scientific Educational Centre 'Nanotechnologies' of MIPT, and was financially supported by the Ministry of Education and Science of the Russian Federation.

References

1. Schuller J.A., Barnard E.S., Cai W., Jun Y.C., White J.S., Brongersma M.L. *Nat. Mater*., **9**, 193 (2010).
2. Schumacher T., Kratzer K., Molnar D., Hentschel M., Giessen H., Lippitz M. *Nat. Commun*., **2**, 333 (2011).
3. Novotny L., van Hulst N. *Nat. Photon*., **5**, 83 (2011).
4. Bouhelier A., Beversluis M., Hartschuh A., Novotny L. *Phys. Rev. Lett*., **90**, 013903 (2003).
5. Canfield B.K., Husu H., Laukkanen J., Bai B.F., Kuittinen M., Turunen J., Kauranen M. *Nano Lett.*, **7**, 1251 (2007).
6. Renger J., Quidant R., van Hulst N., Novotny L. *Phys. Rev. Lett*., **104**, 046803 (2010).
7. Utikal T., Stockman M.I., Heberle A.P., Lippitz M., Giessen H. *Phys. Rev. Lett*., **104**, 113903 (2010).
8. Pacifici D., Lezec H.J., Atwater H.A. *Nat. Photon*., **1**, 402 (2007).
9. MacDonald K.F., Samson Z.L., Stockman M.I., Zheludev N.I. *Nat. Photon*., **3**, 55 (2009).
10. Park I.Y., Kim S., Choi J., Lee D.H., Kim Y.J., Kling M.F., Stockman M.I., Kim S.W. *Nat. Photon*., **5**, 677 (2011).
11. Fomichev S.V., Popruzhenko S.V., Zaretsky D.F., Becker W. *J. Phys. B*., **36**, 3817 (2003).
12. Lippitz M., Dijk M., Orrit M. *Nano Lett.*, **5**, 799 (2005).
13. Hanke T. et al. *Nano Lett*., **12**, 992 (2012).
14. Melentiev P.N., Zablotskiy A.V., Lapshin D.A., Sheshin E.P., Baturin A.S., Balykin V.I. *Nanotechnol.*, **20**, 235301 (2009).
15. Boyd R.W. *Nonlinear Optics* (London: Acad. Press, 2003).
16. Burns W.K., Bloembergen N. *Phys. Rev. B*, **4**, 3437 (1971).
17. Johnson P.B., Christy R.W. *Phys. Rev. B*, **6**, 4370 (1972).
18. Rakic A.D. *Appl. Opt*., **34**, 4755 (1995).
19. Afanasiev A.V. et al. *J. Opt. Technol*., **78**, 537 (2011).
20. Bityurin N. et al. *Appl. Phys. A*, DOI:10.1007/s00339-012-7213-y.
21. Reintjes J.F. *Nonlinear Optical Parametric Processes in Liquids and Gases* (Orlando, Florida: Acad. Press, 1984).
22. Xu T., Jiao X., Blair S. *Opt. Express*, **17**, 23582 (2009).
23. Mie G. *Ann. Phys.*, **25**, 377 (1908).
24. Klimov V.V. *Nanoplazmonika* (Nanoplasmonics) (Moscow: Nauka, 2009) Sect. 12.2.
25. Nakanishi T., Tamayama Y., Kitano M. *Appl. Phys. Lett*., **100**, 044103 (2012).
26. Castro-Lopez M., Brinks D., Sapienza R., van Hults N.F. *Nano Lett*., **11**, 4674 (2011).
27. Varnavski O.P. et al. *J. Phys. Chem. B*, **107**, 3101 (2003).

28. Mohamed M.B., Volkov V., Link S., El-Sayed M.A. *Chem. Phys. Lett*., **317**, 517 (2000).
29. Dulkeith E., Niedereichholz T., Klar T.A., Feldmann J., von Plessen G., Gittins D.I., Mayya K.S., Caruso F. *Phys. Rev. B*, **70**, 205424 (2004).
30. Boyd G.T., Yu Z.H., Shen Y.R. *Phys. Rev. B*, **33**, 7923 (1986).
31. Bouhelier A., Bachelot R., Lerondel G., Kostcheev S., Royer P., Wiederrecht G.P. *Phys. Rev. Lett*., **95**, 267405 (2005).
32. Melentiev P.N., Afanasiev A.E., Kuzin A.A., Zablotskiy A.V., Baturin A.S., Balykin V.I. *Opt. Express*, **9**, 22743 (2011).
33. Melentiev P.N., Afanasiev A.E., Kuzin A.A., Zablotskii A.V., Baturin A.S., Balykin V.I. *Zh. Eksp. Teor. Fiz.*, **142**, 211 (2012) [*JETP*, **115**, 185 (2012)].
34. Melentiev P.N., Konstantinova T.V., Afanasiev A.E., Kuzin A.A., Baturin A.S., Balykin V.I. *Opt. Express*, **20** (17), 19474 (2012).